

PAPER • OPEN ACCESS

## Using Lorentz forces to control the distribution of bubbles in a vertical tube filled with liquid metal

To cite this article: S Heitkam *et al* 2017 *IOP Conf. Ser.: Mater. Sci. Eng.* **228** 012008

View the [article online](#) for updates and enhancements.

### Related content

- [Local symmetry in liquid metals probed by x-ray absorption spectroscopy](#)  
Fabio Iesari and Andrea Di Cicco
- [Steady foam states](#)  
P. Licinio and J. M. A. Figueiredo
- [Letters](#)

# Using Lorentz forces to control the distribution of bubbles in a vertical tube filled with liquid metal

S Heitkam<sup>1</sup>, S Tschisgale<sup>2</sup>, B Krull<sup>2</sup>, T Wetzels<sup>3</sup>, E Baake<sup>4</sup> and J Fröhlich<sup>2</sup>

<sup>1</sup> Technische Universität Dresden, Institut für Verfahrenstechnik und Umwelttechnik, D-01062 Dresden, Germany

<sup>2</sup> Technische Universität Dresden, Institut für Strömungsmechanik, D-01062 Dresden, Germany

<sup>3</sup> Institute of Thermal Process Engineering, Karlsruhe Institute of Technology, Kaiserstr. 12, Karlsruhe D-76131, Germany

<sup>4</sup> Institute of Electrotechnology, Leibniz University of Hanover, Wilhelm-Busch-Str. 4, Hannover D-30167, Germany

E-mail: [sascha.heitkam@tu-dresden.de](mailto:sascha.heitkam@tu-dresden.de)

**Abstract.** In this work, a method to increase the residence time of bubbles in tubes or pipes filled with liquid metal is investigated. Imposing a horizontal electric current and a perpendicular horizontal magnetic field generates an upward-directed Lorentz force. This force can counteract gravity and cause floating of bubbles. Even with homogeneous electric fields these float in the mean but fluctuate randomly within the swarm due to mutual interactions. In the present case the cylindrical shape of the container furthermore creates inhomogeneous electric currents and an inhomogeneous force distribution resulting in a macroscopic convection pattern stirring the bubbles and further homogenising the spatial distribution of the bubbles.

## 1. Introduction

An innovative technique for the production of hydrogen is the direct thermal cracking of methane into carbon and hydrogen. This can be achieved by introducing methane bubbles into tubes filled with liquid tin which serves as a heat transfer medium. The reaction takes place above 600°C but is much faster for higher temperatures. High temperatures, however, pose technical problems such as difficulties of handling the process and devising suitable materials for the construction of the apparatus. Another strategy is to work with somewhat lower temperatures but to increase the residence time of the bubbles by an appropriate amount to accommodate the slower reaction.

At KIT, an experimental facility including a bubble column reactor with molten tin as liquid medium has been developed and constructed in order to prove the feasibility of the concept. Several experimental campaigns have been run, during which parameters like gas volume flow rate, temperature and feed gas dilution were investigated [1, 2]. A major finding is the strong influence of the bubble residence time on the methane conversion. The residence time is limited by the strong acceleration of the gas bubbles in the liquid metal. On the other hand, this density difference is a major advantage of the process, as it facilitates the separation of the solid



carbon produced. Therefore, additional measures which can resolve this conflict would be highly welcome.

To get an idea about the bubble dynamics in the experimental bubble column reactor additional numerical simulations were conducted in Hannover. In these studies, residence times for different volume flow rates and initial bubble sizes including slug flows were determined. To increase the efficiency, installations like packed beds, variation of multiple inlets including coalescence studies were done. Another aspect, the influence of an electromagnetic field with the potential of electromagnetic stirring to split bubbles into blebs, were numerically explored as well.

The option investigated in the present paper is to increase the well time by means of electromagnetic fields. In earlier simulations this was demonstrated for bubbles in liquid aluminum [3]. A horizontal electric and a perpendicular, horizontal magnetic field result in a Lorentz force pointing upwards and counteracting gravity. Further investigation of the floating state [4] revealed, that around each bubble, a swirling velocity field is induced. The interaction of these fields generates a global stirring motion homogenising the spatial distribution of the bubbles.

In the present work this concept is adapted to the bubble column reactor for hydrogen production investigated experimentally. Most importantly, a cylindrical domain is used here since this is an essential feature of the experiment. The cylindrical geometry of the electrodes results in an inhomogeneous distribution of the electric current thus resulting in an inhomogeneous Lorentz force and a macroscopic mean velocity field. Goal of this work is to evaluate the movement of liquid metal and bubbles in such an electromagnetic field and to provide first information about the suitability for an industrial process.

## 2. Numerical Method

### 2.1. Euler-Lagrange approach

The simulations were carried out with the in-house code PRIME [5]. It solves the incompressible Navier-Stokes equations

$$\frac{\partial \mathbf{u}}{\partial t} = -(\mathbf{u} \cdot \nabla) \mathbf{u} + \frac{1}{\rho_f} \nabla p + \nu \nabla^2 \mathbf{u} + \frac{1}{\rho_f} \mathbf{j} \times \mathbf{B} + \mathbf{f}_{IBM} \quad (1)$$

$$\nabla \cdot \mathbf{u} = 0 \quad (2)$$

on a staggered Cartesian grid and employs a Runge-Kutta three-step low-storage method with pressure correction for time integration.

The bubbles are geometrically resolved and equations of motion for velocity and rotation are solved for each individual bubble. The bubbles are assumed mono-disperse and spherical, with a no-slip condition applied at their surface [6]. An immersed boundary method described below is used to couple the disperse and the continuous phase. In case of bubble collision, additional forces are added to the equation of motion of the bubbles, in order to model the physical collision process [7].

### 2.2. Immersed boundary method

Besides the bubbles, the immersed boundary method is also employed to represent the walls of the cylindrical fluid domain within a hexagonal Cartesian grid. This facilitates grid generation tremendously. Each embedded boundary  $\Gamma$ , whether bubble surface or container wall, is represented by a finite set of Lagrangian marker points evenly distributed over  $\Gamma$  to accomplish the coupling to the surrounding fluid. At the position of each marker point  $\mathbf{x}_m \in \Gamma$  an artificial force  $\mathbf{f}_{IBM}$  is added to the Navier-Stokes equation, as shown in (1). This source term is

determined by the so-called direct forcing approach [8, 9, 10]

$$\bar{\mathbf{f}}_{IBM} = \frac{1}{\Delta t} \int_{t_{n-1}}^{t_n} \mathbf{f}_{IBM} dt = \frac{\mathbf{u}_F^n - \tilde{\mathbf{u}}}{\Delta t}, \quad (3)$$

where  $\bar{\mathbf{f}}_{IBM}$  is the average IBM force applied over the discrete time interval  $\Delta t = t_n - t_{n-1}$ . In equation (3) the velocity  $\tilde{\mathbf{u}}$  is a shorthand for

$$\tilde{\mathbf{u}} = \mathbf{u}^{n-1} + \int_{t_{n-1}}^{t_n} \mathbf{rhs} dt \quad , \quad (4)$$

with  $\mathbf{rhs}$  representing the right-hand side of the momentum balance (1), excluding  $\mathbf{f}_{IBM}$ , so that the preliminary fluid velocity  $\tilde{\mathbf{u}}$  is obtained without accounting for the effect of the immersed boundary.

Due to the no-slip condition the fluid velocity at a marker position is equal to the velocity of the interface, i.e.  $\mathbf{u}_F^n = \mathbf{u}(\mathbf{x}_m, t^n)$ . In case of the container walls  $\mathbf{u}_F^n$  vanishes. In case of the bubbles, their surface is represented by 1259 Lagrangian marker points. At these points the no-slip boundary condition is imposed by  $\bar{\mathbf{f}}_{IBM}$  in (1) and  $\mathbf{u}_F^n$  obtained from the equation of motion of the bubble. The counteracting forces  $-\bar{\mathbf{f}}_{IBM}$  at these markers are collected and introduced in the equations of motion of the bubble.

### 2.3. Magnetohydrodynamics

To represent magnetohydrodynamic effects in the simulation, an electric current density  $\mathbf{j}$  and a magnetic field strength  $\mathbf{B}$  have to be determined in (1). The magnetic susceptibility of liquid tin, methane and air are all close to zero. Thus, interfaces of these materials do not alter the magnetic field. Also the magnetic Reynolds number is low, so that the magnetic field  $\mathbf{B} = B_0 \mathbf{e}_y$  can be assumed constant in space and time.

The electric conductivity of liquid tin,  $\sigma_f$ , on the contrary, is much higher compared to methane, or hydrogen or air. Hence, bubbles of conductivity  $\sigma_g \ll \sigma_f$  alter the electric current. Electric induction has to be taken into account as well. The electric current density, then is given by

$$\mathbf{j} = \sigma_{el}(\mathbf{u} \times \mathbf{B} - \nabla \phi) \quad , \quad (5)$$

and charge conservation  $\nabla \cdot \mathbf{j} = 0$  results in a Poisson equation for the electric potential

$$\nabla^2 \phi = \nabla \cdot (\mathbf{u} \times \mathbf{B}) \quad . \quad (6)$$

which is numerically solved. The boundary condition at the bubble interfaces are imposed by scaling the electric conductivity  $\sigma_{el} = \alpha \sigma_f$  with  $\alpha \in [0, 1]$ , a phase marker function derived from a cut-cell algorithm [5]. At the surface of the tube, the marker points are employed to impose the correct value for the wall-normal electric current using the Neumann condition  $\partial \phi / \partial n = j / \sigma_f$  with  $j = j_0$  at one electrode,  $j = -j_0$  at the other electrode and  $j = 0$  otherwise. Once  $\phi$  is known from (6),  $\mathbf{j}$  is obtained from (5).

## 3. Setup

The material parameters for the simulation are derived from [11] and references therein. The considered temperature  $1000^\circ C$  is within the range  $900^\circ C$  to  $1175^\circ C$  used in the experiments at KIT. Higher temperatures allow for higher production rate but are more difficult to handle, because the magnet might have to be cooled and the material of the electrode has to withstand it.

**Table 1.** Parameters for the simulation. Material parameters are derived from [11] and references therein.

Parameter	Symbol	Value
Temperature	$T$	$1000^{\circ}C$
Density	$\rho_f$	$6500 \text{ kg/m}^3$
Viscosity	$\nu_f$	$1.1 \cdot 10^{-7} \text{ m}^2/\text{s}$
El. conductivity	$\sigma_f$	$1.3 \cdot 10^6 \text{ S/m}^{-1}$
Tube diameter	$D$	$16 \text{ mm}$
Tube height	$H$	$16 \text{ mm}$
Bubble diameter	$D_b$	$2 \text{ mm}$
Number of bubbles	$N_b$	50
Surface tension	$\gamma$	$0.5 \text{ N/m}$
Mag. field strength	$B_0$	$0.1 \text{ T}$
El. current density	$j_0$	$0.5 \text{ A/mm}^2$

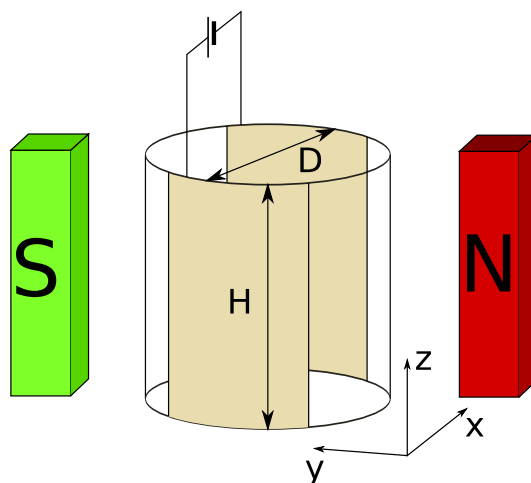


**Figure 1.** Setup of the investigation showing the tube with electrodes and magnets together with the coordinate system employed.

The geometrical setup is shown in figure 1. Top and bottom are non-conducting solid walls. The tube is filled with liquid tin, as in the experiments and has a diameter of 16 mm and a height of 16 mm as well. This is smaller than the experiment at KIT to limit computational resources. In an industrial process, the height and the diameter would be much larger, but important mechanisms can also be evaluated with this reduced size. Each of the electrodes covers the full height and 90 degrees of the circumference. The magnetic poles are placed perpendicularly to the electrodes.

At the initial state of the bubble-laden simulations 50 gas bubbles of 2 mm diameter were placed at random positions within the tube and allowed to freely propagate under the influence of the various forces.

## 4. Results

### 4.1. Static channel

First, computations in matlab<sup>®</sup> were conducted to determine the current density alone in the channel filled with stagnant material of constant conductivity, to understand the Lorentz force distribution in the present setup with curved electrodes. This is reported in figure 2a displaying the  $x$ -component of the current density. It shows significant minima close to the insulating parts of the tube surface. Close to the border of the electrodes strong maxima appear. This feature results from the electric boundary condition at the electrodes. For comparison, a case with constant voltage imposed at the electrodes, i.e.  $\phi = \pm\phi_0$ , was computed as well and is presented in figure 2b. For the following simulations, constant normal electric current at the

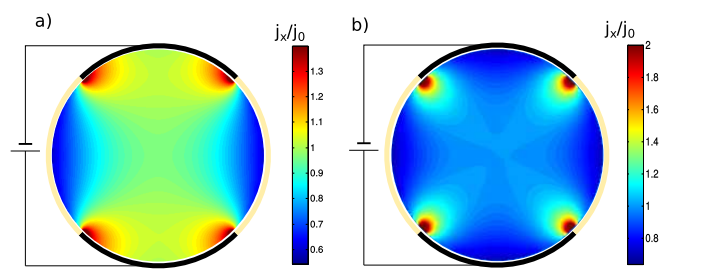


**Figure 2.** Theoretical current distribution in a cross section of the tube, filled with stagnant material of constant conductivity. The  $x$ -direction of the electric current is shown for two different boundary conditions at the electrodes. a) Constant normal current, b) constant potential. The  $x$ -direction is vertical in these graphs.

electrodes (Figure 2a) was imposed. Note, that the boundary condition only enforces the normal component, not the total value. At the apex of the electrode, the  $x$ -component equals the normal value, which is set by the boundary condition. At the rim, the electrode is tilted up to 45 degree. Thus, the local area of the electrode is larger than the corresponding projection of the electrode area perpendicular to the  $x$ -direction. Due to conservation of charge, the current density in  $x$ -direction has to be approximately  $\sqrt{2} \approx 1.4$  times larger than the normal current at the electrode.

### 4.2. Single-phase flow

As a next step, the single-phase flow was computed with the code described above. The  $x$ -component of the electric current directly determines the vertical Lorentz force  $f_{L,z} = j_x B_0$ , so that the vertical velocity reflects the inhomogeneity of the electric current. The vertical velocity, averaged over the height of the tube, is shown in figure 3. Although the flow is not homogeneous in  $z$ -direction due to the top and bottom wall this figure provides an impression of the fluid flow generated by the Lorentz force with averaged values reaching  $\langle w \rangle_z \approx 0.04$  m/s. This yields a Reynolds number in magnitude of

$$Re = \frac{\langle w \rangle_z D}{\nu_f} \approx 5000 \quad . \quad (7)$$

The velocity field was not averaged in time. The small irregularities and asymmetries visible in this graph reflect the fact that the instantaneous flow exhibits substantial turbulence. This issue is not discussed further here, because the introduction of bubbles changes the flow substantially.

Figure 4 shows the  $x$ -component of the electric current in the single-phase flow. It is obvious that this field is more homogeneous than the current density shown in figure 2a. This is for two

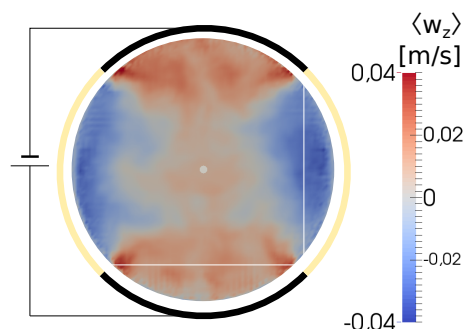


**Figure 3.** Upward velocity averaged over the height of the tube,  $\langle w \rangle$  .

reasons. First, the motion of the liquid metal is attenuated and homogenised by viscous effects. Second, the fluid moving in a direction different from the magnetic field itself generates electric current as described by (5). The load factor  $K$  relates the externally applied electric field  $j_0/\sigma_f$  to the induced electric field  $\langle w \rangle_z B_0$

$$K = \frac{j_0}{\sigma_f} \frac{1}{\langle w \rangle_z B_0} \approx 0.96 \quad . \quad (8)$$

A load factor close to one means, that the induced electric currents are of the same magnitude as the applied ones. Regions of high electric current show high vertical Lorentz forces and, in turn, high vertical velocities. The vertical movement generates high induced electric fields counteracting the applied ones. This feed loop leads to more balanced distribution of  $j_x$  with smaller amplitude shown in figure 4.

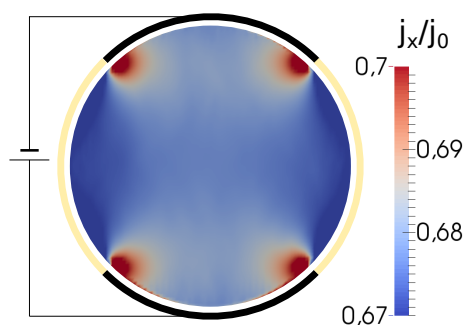


**Figure 4.** Normalised horizontal distribution of the  $x$ -component of the electric current density, averaged over the height of the tube.

#### 4.3. Bubble distribution

Bubbles distributed in the tube experience several effects, such as buoyancy, drag force, pressure gradient and collision forces. Earlier simulations of the present authors of bubbles in a rectangular container [3] used that the vertical Lorentz force generates an upside-down pressure gradient  $j_0 B_0$  that counteracts buoyancy  $\rho_f g$  and causes floating of bubbles. For floating, the

Lorentz force has to overcompensate gravity by 1/3 [12] yielding

$$j_0 B_0 = \frac{4}{3} \rho_f g \quad (9)$$

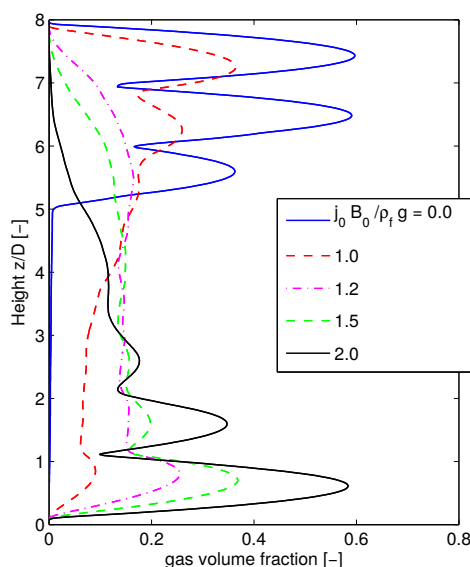


**Figure 5.** Mean bubble volume fraction over height obtained from averaging over time and horizontal directions in the considered tube with horizontal electric and magnetic fields. The latter is perpendicularly oriented to the electric field.

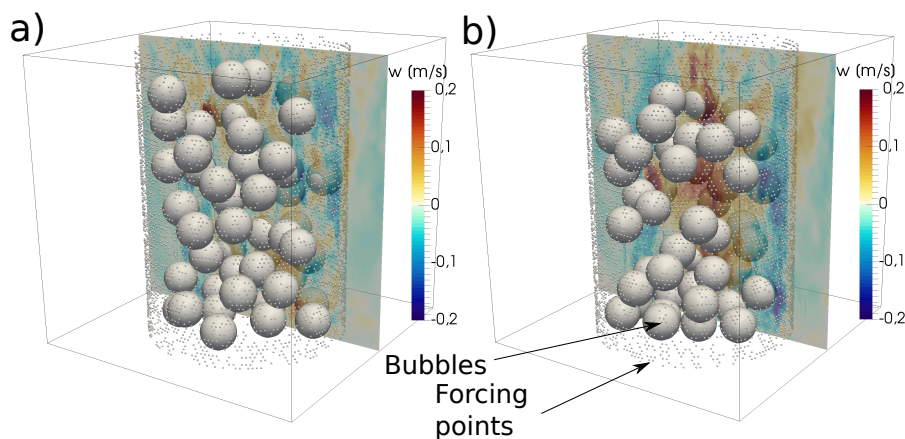


**Figure 6.** Snapshot of bubble distribution and vertical velocity component in a vertical plane off the axis. a)  $j_0 B_0 / \rho_f g = 1.2$ , b)  $j_0 B_0 / \rho_f g = 1.5$ . The small white points are forcing points on the cylindrical container surface serving to impose the boundary conditions. Only a small subset of these points is shown not to hide the interior of the domain.

As demonstrated in figure 5 this is also true for a round container. Without electromagnetic field the bubbles agglomerate at the top of the container. The undulating shape of the curve

results from the fact that the top wall imposes a certain structure on the position of bubbles. With increasing field strength, the bubbles become mobilised, float and even collect at the bottom of the domain if the Lorentz force is substantially exceeding gravity. A stable state with mostly floating irregularly moving bubbles is achieved for  $j_0 B_0 / \rho_f g \approx 1.2$ , corresponding to an overcompensation of gravity by about 20%.

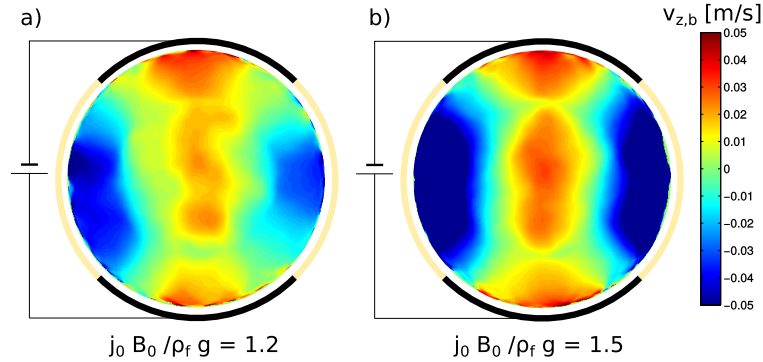


**Figure 7.** Vertical velocity of bubbles averaged over time and vertical direction for different values of applied electric field strength. a)  $j_0 B_0 / \rho_f g = 1.2$ , b)  $= 1.5$ , respectively.

For the two cases depicted in figure 6a and 6b, the vertical velocity of the bubbles was averaged over height and in time yielding the data in figure 7. The resulting motion reflects the distribution of the Lorentz force and of the vertical fluid velocity. The fluid velocity of the single-phase flow exhibits a similar magnitude (cf. figure 3). This suggests, that the bubbles are not propelled by their interaction with the electromagnetic field but that they are transported by the macroscopic flow structure of the liquid metal.

## 5. Discussion

To reduce the complexity, the present simulations did not account for bubble deformation and coalescence. When the bubbles agglomerate, coalescence might occur, since presumably no surface active agent is present. However, in the floating state, collisions are less frequent and coalescence should be negligible due to the low contact times [13].

As pointed out in section 4.1 the structure of the inhomogeneity of the electric current highly depends on the electric boundary condition. In the present case, constant normal current is imposed at the walls. Constant potential at each electrode results in a more homogeneous current density and, hence, a more homogeneous Lorentz force in the empty tube. A constant potential boundary condition, however, has a major problem, because in cross sections with many bubbles the average resistance is higher resulting in lower electric current. This, in turn, reduces the Lorentz force near bubble clusters, so that no stable bubble distribution is to be expected. Consequently, in industrial applications a constant-current boundary condition has to be targeted. This is possible by splitting the electrode in parts imposing a constant current at each part. Measuring the corresponding potential could also allow measurement of the bubble distribution by impedance tomography.

The goal of the present study is to improve the generation process of hydrogen. The efficiency can be evaluated, roughly, by comparing the energy stored in the produced hydrogen,  $P_H$ , and the energy spent for imposing the electric current,  $P_j$ , giving  $\eta = P_H / P_j$ . The electric energy consumption per reactor volume depends on the electric current density. With a stronger magnetic field, a smaller electric current is necessary to achieve the floating state. However, magnetic field strengths above  $B_0 = 0.1T$  are presumably difficult to handle in practical applications. This results in an electric power consumption of approximately  $10^7 W/m^3$  per

reactor volume. The production rate of hydrogen depends largely on the temperature and further parameters of the process and has yet to be assessed. It is clear, that the use of magnetohydrodynamic forces requires energy input which has to be justified by improved output of the process. This could be in the form of increased hydrogen reaction rates, but other processes might be considered as well, where the additional value is brought by the quality of the products, for example, so that the price for the energy is of lower importance. Further work is required to conclusively assess the potential of the "zero-gravity" option in liquid metal reacting bubbly flows.

### Acknowledgements

The support of the Helmholtz Alliance LIMTECH via the project A5 and a Seed Grant in 2015, as well as the support of the German Research Foundation (HE 7529/1-1) is gratefully acknowledged. Computation time was provided by ZIH at TU Dresden.

### References

- [1] Geißler T, Plevan M, Abánades A, Heinzl A, Mehravaran K, Rathnam R, Rubbia C, Salmieri D, Stoppel L, Stückrad S, Weisenburger A, Wenninger H and Wetzel T 2015 *Int. J. Hydrogen Energy* **40** 14134–14146
- [2] Geißler T, Abánades A, Heinzl A, Mehravaran K, Müller G, Rathnam R, Rubbia C, Salmieri D, Stoppel L, Stückrad S, Weisenburger A, Wenninger H and Wetzel T 2016 *Chem. Eng. J.* **299** 192–200
- [3] Heitkam S, Schwarz S, Santarelli C and Fröhlich J 2013 *Eur. Phys. J. Special Topics* **220** 207–214
- [4] Heitkam S 2014 *Manipulation of liquid metal foam with electromagnetic fields: a numerical study* Ph.D. thesis Institut für Strömungsmechanik, TU Dresden
- [5] Kempe T and Fröhlich J 2012 *J. Comput. Phys.* **231** 3663–3684
- [6] Aland S, Schwarz S, Fröhlich J and Voigt A 2013 *J. Comput. Phys.* **220** 185–194
- [7] Heitkam S, Sommer A, Drenckhan W and Fröhlich J 2017 *Journal of Physics: Condensed Matter* **29** 124005
- [8] Mohd-Yusof J 1997 *Center for Turbulence Research. Ann. Res, Briefs. NASA Ames / Stanford University* 317–327
- [9] Fadlun E A, Verzicco R, Orlandi P and Mohd-Yusof J 2000 *J. Comput. Phys.* **161** 35–60
- [10] Tschisgale S, Kempe T and Fröhlich J 2017 *J. Comput. Phys.* **339** 432–452
- [11] Sharafat S and Ghoniem N 2000 Summary of thermo-physical properties of Sn and compounds of Sn–H, Sn–O, Sn–C, Sn–Li, Sn–Si and comparison of properties of Sn, Sn–Li, Li, Pb–Li Tech. Rep. UCLA-UCMEP-00-31 University of California
- [12] Lenov D and Kolin A 1954 *J. Chem. Phys.* **22** 683–688
- [13] Schwarz S, Tschisgale S and Fröhlich J 2013 Modeling of bubble coalescence in phase-resolving simulations by an immersed boundary method Int. Conf. Multiphase Flows, Paper 750